Arch Appl Mech (2015) 85:1209–1223
DOI 10.1007/s00419-014-0937-8

SPECIAL

Aristotelis E. Charalampakis

The response and dissipated energy of Bouc–Wen hysteretic model revisited

Received: 7 October 2013 / Accepted: 11 August 2014 / Published online: 26 November 2014

Abstract In this work, the response and dissipated energy of the well-known Bouc–Wen model are examined in detail. New analytical and numerical solutions are derived using a generic model formulation without any parameter constraints. Theoretical issues, such as the inexistence of an elastic domain and the evaluation of the residual deformation after a loading–unloading cycle are addressed by means of analytical equations. This work capitalizes on previous findings by the author and recent advancements in the field to target both theoretical and numerical implementation issues.

Keywords Bouc–Wen · Hysteresis · Plasticity · Dissipated energy

1 Introduction

Hysteresis is a phenomenon observed across many scientific fields ranging from mechanics, materials, and magnetism to biology, sociology, and economics. According to Visintin [1], *hysteresis* = *rate-independent memory effect*. Thus, the future state of a hysteretic system depends not only on its current state but also on its past history.

A popular and versatile hysteretic model is the Bouc–Wen model [2,3]. It has been applied in many problems, including the response of beam members [4,5], concrete walls [6], masonry walls [7], seismic isolation devices [8,9], wood joints [10], caisson foundations [11], magnetorheological fluid dampers [12,13], as well as more specific applications such as the stick-slip phenomena in elevator guide rails [14], or the restoring force in seat suspension systems [15], to name a few. A survey on the implementations of the Bouc–Wen model can be found in the work of Ismail et al. [16].

Being phenomenological, the Bouc–Wen model is able to describe complex responses using even single-degree-of-freedom (SDoF) systems. These can be embedded into large-scale models or used in finite element analysis [17–19]. The complex internal mechanism producing the overall hysteresis is not examined at all. Obviously, the response and dissipated energy of such a system is of great interest. A previous study examined the model and produced certain analytical solutions [20], useful e.g., in the derivation of a modified Bouc–Wen model compatible with Drucker's and Il'iushin's postulates of plasticity [21]. The study [20] is extended herein in the following ways: (a) A popular generic formulation of the model is used, without any parameter constraints, (b) Additional analytical solutions are derived, (c) Certain theoretical issues are addressed, such as the inexistence of an elastic domain, the evaluation of the residual deformation after a loading-unloading cycle, the relation of the derived solutions with other results found in the literature. (d) Detailed implementation guidelines are presented in the Appendices, including worked examples and numerical algorithms.

A. E. Charalampakis (✉)
National Technical University of Athens (NTUA), Athens, Greece
E-mail: aristotelis.charalampakis@gmail.com; achar@mail.ntua.gr
Tel: +30 210 7721657
URL: http://www.charalampakis.info/

After the model formulation, the remainder of the study is arranged in two major sections, treating the evaluation of the response and dissipated energy, respectively. The state of the art in each topic is described in the introduction of the corresponding section.

2 Model formulation

The Bouc–Wen model captures the true hysteresis by means of auxiliary hysteretic variables which follow suitable differential equations with zero initial conditions. For the case of a SDoF system, and following the notation in [22], the hysteresis is given by:

$$\Phi(t) = a\,k\,x(t) + (1-a)\,D\,k\,z(t) \tag{1}$$

where, $0 < a < 1, k > 0, D > 0, x(t)$ is the time history of the input variable and $z(t)$ is a dimensionless hysteretic variable which is governed by the following differential equation:

$$\dot{z} = D^{-1}\left(A\dot{x} - \beta\,|\dot{x}|\,|z|^{n-1}\,z - \gamma\dot{x}\,|z|^{n}\right) \tag{2}$$

or, simply:

$$\dot{z} = D^{-1}\left(A - (\beta\,\mathrm{sgn}(z\,\dot{x}) + \gamma)\,|z|^{n}\right)\dot{x} \tag{3}$$

in which $n > 0$ and $sgn(\cdot)$ is the signum function. It is noted that nowadays the notation varies from paper to paper, and in several cases, the parameters β and γ are interchanged, e.g., [20]. In the context of structural mechanics, x is usually the displacement, k the initial (elastic) stiffness, a the ratio of post to pre-yield stiffness, D is the yield displacement, and n is a dimensionless exponential parameter which governs the abruptness of transition between pre- and post-yield response. The dimensionless parameters A, β, γ control the shape and size of the hysteretic loop. The parameter D can be omitted from Eqs. (1)–(3), in which case z obtains units of length and may be referred to as the *hysteretic displacement*. However, using dimensionless hysteretic variables is usually advantageous, since they are more meaningful with respect to the level of the plastification of the system. Based on Eq. (1), the Bouc–Wen model can be visualized as two springs connected in parallel, i.e., a linear elastic and a hysteretic spring, with $\Phi^{el}(t) = a\,k\,x(t)$ and $\Phi^{h}(t) = (1-a)\,D\,k\,z(t)$.

3 Model response

3.1 Literature survey

Regarding the model response, Wen claims that when $n = 1$, the $x - z$ curve "is of exponential type" [3]. However, he does not provide results. Dominguez et al. [23] provide results for $n = 1$ and $n = 2$, but some integration constants are missing [16]. Ikhouane and Rodellar analyze the model using "instrumental functions" [22]. This approach will be investigated in detail in a subsequent paragraph. Recently, analytical relations for the response were derived for a Bouc–Wen model with well-defined mechanical properties [20]. These properties are ensured by imposing specific parameter constraints, which are not necessary from a mathematical point of view. Thus, analytical relations will be produced in the next section, in their most general form, for the formulation of Eqs. (1) and (3).

3.2 Model classification

In [16,22], several classes of bounded-input, bounded-output (BIBO) stable Bouc–Wen models have been defined. We will focus in classes I and II (in which $A > 0$, Table 1), as these usually represent the behavior of actual systems, although the derived relations may be also applicable to non-BIBO-stable models. Cases III and IV, in which $A < 0$, can be analyzed using the same methodology, if needed. In case V ($A = 0$), the system exhibits linear response since $z(0) = 0$ and hence $dz/dx = 0$ due to Eq. (4). This case will be ignored altogether.

Table 1 BIBO stable Bouc–Wen model classification [16,22]

Parameter constraints	Class
$A > 0$ and $\beta + \gamma > 0$ and $\beta - \gamma \geq 0$	I
$A > 0$ and $\beta - \gamma < 0$ and $\beta \geq 0$	II

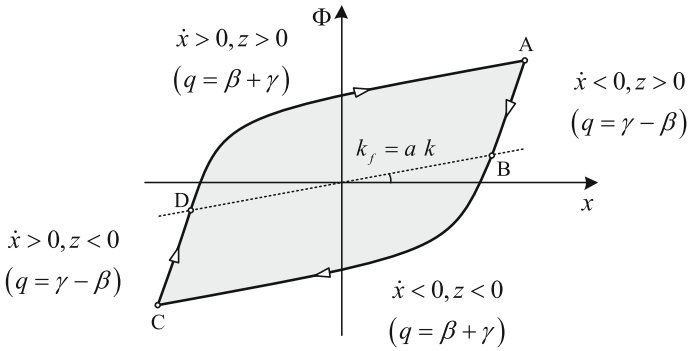

Fig. 1 Response of a SDoF Bouc–Wen model under cyclic excitation

3.3 Solution for arbitrary n

The hysteresis produced by the Bouc–Wen model is rate independent. Equation (3) can be written in the form:

$$\frac{dz}{dx} = D^{-1}\left(A - (\beta\ \mathrm{sgn}\,(z\ \dot{x}) + \gamma)\ |z|^n\right) \tag{4}$$

where $\dot{x}$ within the signum function serves only as an indicator of movement direction. Thus, the response of Bouc–Wen model can be divided into four segments (AB, BC, CD, and DA) depending on the sign of $\dot{x}$ and z (Fig. 1).

Assuming $A \neq 0$ and $q = \beta\ \mathrm{sgn}\,(z\ \dot{x}) + \gamma$, constant for the transition under examination, i.e., there is no transition between branches, the indefinite integral of Eq. (4) is given by Gauss' hypergeometric function ${}_2F_1\,(\cdot)$. Accounting for initial conditions, one obtains:

$$\frac{x - x_0}{D} = \frac{z}{A}\ {}_2F_1\left(1, \frac{1}{n}, 1 + \frac{1}{n}; \frac{q}{A}\ |z|^n\right)\Bigg|_{z_0}^{z} \tag{5}$$

Equation (5) is valid even when $q = 0$, i.e., when $\gamma = \beta$ and $\mathrm{sgn}\,(z\ \dot{x}) = -1$, in which case it is simplified as:

$$\frac{x - x_0}{D} = \frac{z - z_0}{A} \tag{6}$$

Note that Eq. (6) is independent of n.

Equation (5) explicitly provides the input x of the hysteretic operator in terms of its output z. Solving Eq. (5) for z does not seem to be possible for an arbitrary value of n. Analytical solutions will be produced for $n = 1$ and $n = 2$ in the subsequent sections.

The lack of a generic inverse relation $z = f\,(x)$ is not so important, because the numerical evaluation of z can be performed very efficiently. An inspection of Eq. (4) shows that the hysteretic parameter z is a continuous and strictly monotonic function of x. Thus, there exists a single root, if any, of Eq. (5) within a bracketed range. The root can be evaluated efficiently by bisection-type methods [20]. In particular, the Van Wijngaarden–Dekker–Brent method exhibits excellent performance [20,24]. In order to define a bracket, the maximum possible value of z is useful. Assuming loading conditions and setting $dz/dx = 0$ in Eq. (4), this value is:

$$z_{\max} = \sqrt[n]{\frac{A}{\beta + \gamma}} \tag{7}$$

Note that $A/(\beta+\gamma) > 0$ for classes I and II, as they exhibit softening behavior; thus, $z_{\max}$ is real. Alternatively, other root-finding methods which do not require root bracketing may be applied. A worked example, demonstrating loop tracing with arbitrary n, is provided in the Appendix A.

Note that, considering the hypergeometric function ${}_2F_1\,(a, b, c; w)$, point $(1, 0)$ is singular in the complex plane and the limit needs to be evaluated as $w \to 1^-$. Proper evaluation techniques are given in the Appendix C. In particular, when loading in either direction, root bracketing is attempted with maximum value of $|z|$ equal to $z_{\max} - \varepsilon$, where ε is a sufficiently small number. If root bracketing fails, then the system has yielded fully and $z = \pm z_{\max}$. When unloading, if root bracketing fails then there is a segment transition, i.e., from AB to BC or from CD to DA, and the response needs to be evaluated in two steps.

3.4 Solution for n = 1

For $n = 1$, Eq. (5) is simplified as:

$$\frac{x - x_0}{D} = -\frac{\operatorname{sgnz}}{q}\left(\ln\left(A - q\,|z|\right) - \ln\left(A - q\,|z_0|\right)\right) \tag{8}$$

where, $\ln(\cdot)$ is the natural logarithm and $\operatorname{sgnz} = \operatorname{sgn}(z + z_0)$, the sign of the hysteretic variable in the transition under examination, i.e., $\operatorname{sgnz} = 1$ for DA and AB branches; $\operatorname{sgnz} = -1$ otherwise. This algorithmic manipulation is necessary since occasionally z or z_0 may be zero. Equation (8) is solved for z analytically:

$$z = \frac{\operatorname{sgnz}\,A + \left(q\,z_0 - \operatorname{sgnz}\,A\right) e^{-\frac{\operatorname{sgnz}\,q\,(x - x_0)}{D}}}{q} \tag{9}$$

3.5 Solution for n = 2

For $n = 2$, Eq. (5) is simplified as:

$$\frac{x - x_0}{D} = \frac{\operatorname{atanh}\left(\sqrt{\frac{q}{A}}z\right) - \operatorname{atanh}\left(\sqrt{\frac{q}{A}}z_0\right)}{\sqrt{q\,A}} \tag{10}$$

where, $\operatorname{atanh}(\cdot)$ is the inverse hyperbolic tangent. Equation (10) is solved for z analytically:

$$z = \frac{\tanh\left(\frac{\sqrt{q\,A}(x - x_0)}{D} + \operatorname{atanh}\left(\sqrt{\frac{q}{A}}z_0\right)\right)}{\sqrt{\frac{q}{A}}} \tag{11}$$

where, $\tanh(\cdot)$ is the hyperbolic tangent. In the previous relations, complex numbers may be involved but the result is real. The relation $\operatorname{atanh}(iy)/i = \operatorname{atan}(y)$, $i = \sqrt{-1}$ can be used to simplify the equations.

3.6 Relation with other results in the literature

Regarding the limit cycle, Ikhouane and Rodellar analyzed a normalized version of the Bouc–Wen model using "instrumental functions" [22]. In particular, for $w \geq 0$ ($\sigma \geq 1/2$ is always assumed):

$$\varphi^-_{\sigma,n}(w) = \int_0^w \frac{du}{1 + (2\sigma - 1)\,u^n} \tag{12}$$

$$\varphi^+_{\sigma,n}(w) = \int_0^w \frac{du}{1 - u^n} \tag{13}$$

while for $w \leq 0$:

$$\varphi^-_{\sigma,n}(w) = \int_0^w \frac{du}{1 - (-u)^n} \tag{14}$$

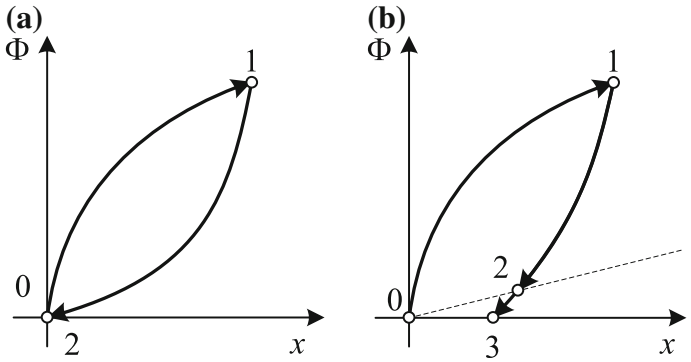

Fig. 2 **a** Supposed closed loading/unloading cycle with no residual deformation **b** actual loading/unloading cycle of Bouc–Wen model. The *dotted line* signifies the response of the linear spring

$$\varphi_{\sigma,n}^{+}(w) = \int_0^w \frac{du}{1 + (2\sigma - 1)(-u)^n} \tag{15}$$

Although these functions are defined explicitly, their use is cumbersome (e.g., the use of tabulated pairs of inputs/results is suggested [22], with linear interpolation in between). Herein, it is noted that the integrals in Eqs. (12)–(15) also have analytical solutions in terms of Gauss' hypergeometric function. In particular, for $w \geq 0$:

$$\varphi_{\sigma,n}^{-}(w) = w\, {}_2F_1\left(1, \frac{1}{n}, 1 + \frac{1}{n}; (1 - 2\sigma)\, w^n\right) \tag{16}$$

$$\varphi_{\sigma,n}^{+}(w) = w\, {}_2F_1\left(1, \frac{1}{n}, 1 + \frac{1}{n}; w^n\right) \tag{17}$$

while for $w \leq 0$:

$$\varphi_{\sigma,n}^{-}(w) = w\, {}_2F_1\left(1, \frac{1}{n}, 1 + \frac{1}{n}; (-w)^n\right) \tag{18}$$

$$\varphi_{\sigma,n}^{+}(w) = w\, {}_2F_1\left(1, \frac{1}{n}, 1 + \frac{1}{n}; (1 - 2\sigma)(-w)^n\right) \tag{19}$$

The use of the hypergeometric function is advantageous, because most software packages either have the function already built-in, or it is easy to program it, as demonstrated in the Appendix C. Finally, the evaluation of the inverse functions can be accomplished to any accuracy with bisection-type methods, in the spirit of the methodology presented previously.

3.7 Inexistence of elastic domain

Regarding the response, Ikhouane et al. analyzed the hysteretic loops produced by the Bouc–Wen model by dividing the response into a linear part, a transition part, and a plastic part [25]. Although clearly stated in [25], it is worth emphasizing that the "linear" part of the response is *almost* linear. The Bouc–Wen model belongs to the class of endochronic models, pioneered by Valanis [26], which discard the notion of a yield surface to describe plasticity [27]. Based on the analytical relations produced herein, one can elaborate on this point.

Suppose there exists a closed loading/unloading cycle of the Bouc–Wen model with no residual deformation (Fig. 2a). The response of the elastic spring is irrelevant in a closed deformation cycle. Regarding the hysteretic spring, employing Eq. (5) for the transitions $0 \to 1$ and $1 \to 2$ (in which $z_1 > 0$) and adding by parts, one obtains:

$${}_2F_1\left(1, \frac{1}{n}, 1 + \frac{1}{n}; \frac{\beta + \gamma}{A} z_1^n\right) = {}_2F_1\left(1, \frac{1}{n}, 1 + \frac{1}{n}; \frac{\gamma - \beta}{A} z_1^n\right) \tag{20}$$

Due to the monotonicity of the branches, Eq. (20) holds only when $\beta = 0$. In this case, the hysteretic spring degenerates into a nonlinear elastic one with a response resembling to an elongated "S".

3.8 Evaluation of residual deformation

If $\beta \neq 0$, then there exists some residual deformation irrespective of the amplitude of the loading, as shown in Fig. 2b. Employing Eq. (5) in the transition $0 \rightarrow 1$ we obtain ($z_0 = 0, x_0 = 0,\ z_1 > 0$):

$$\frac{x_1}{D} = \frac{z_1}{A}\,{}_2F_1\left(1, \frac{1}{n}, 1+\frac{1}{n}; \frac{\beta+\gamma}{A} z_1^n\right) \tag{21}$$

Examining the transition $1 \rightarrow 2$ ($z_2 = 0$):

$$\frac{x_2 - x_1}{D} = 0 - \frac{z_1}{A}\,{}_2F_1\left(1, \frac{1}{n}, 1+\frac{1}{n}; \frac{\gamma-\beta}{A} z_1^n\right) \tag{22}$$

While for the transition $2 \rightarrow 3$ ($z_2 = 0$):

$$\frac{x_3 - x_2}{D} = \frac{z_3}{A}\,{}_2F_1\left(1, \frac{1}{n}, 1+\frac{1}{n}; \frac{\beta+\gamma}{A} |z_3|^n\right) - 0 \tag{23}$$

At point 3, $z_3 < 0$ and the response of the linear spring is the opposite of that of the hysteretic spring. Setting $\Phi = 0$ in Eq. (1) we obtain:

$$z_3 = -\frac{a\, x_3}{(1-a)\, D} \tag{24}$$

By adding Eqs. (21)–(23) by parts and substituting Eq. (24), we obtain an equation relating the value of z_1, i.e., the maximum value of z achieved during loading, obtained from Eq. (21), with the residual deformation x_3. In particular, for $n = 1$, z_1 is given by:

$$z_1 = A\frac{1 - e^{-\frac{(\beta+\gamma)x_1}{D}}}{(\beta+\gamma)} \tag{25}$$

Then, x_3 is given by:

$$x_3 = -\frac{D}{a\,(\beta+\gamma)} \times \left((\alpha-1)\,A + a\ \text{ProductLog}\left(-\frac{(\alpha-1)\,\mathrm{e}^{\frac{1-a}{a}A}\,(A-(\beta+\gamma)\,z_1)\left(1-\frac{(\gamma-\beta)z_1}{A}\right)^{-\frac{\beta+\gamma}{\gamma-\beta}}}{a}\right)\right) \tag{26}$$

where, ProductLog$(\cdot)$ gives the principal solution of Lambert's W function (or Omega function) [28].

Following the aforementioned methodology, we can examine the residual deformation x_3 in a loading/unloading cycle as a function of the loading intensity x_1 (Fig. 3), where we observe that x_3 maybe small but it is nonzero, especially when n is small.

4 Dissipated energy

4.1 Literature survey

The dissipated energy is of great importance in mechanics as it is a direct measure of the damage level in structural elements, especially when they are subjected to inelastic deformations [29]. Usually, the dissipated energy of the Bouc–Wen model is either evaluated numerically or estimated based on the equivalent bilinear system. Recently, analytical relations for the dissipated energy were derived for a Bouc–Wen model under symmetric wave T-periodic input [20]. Herein, the parameter constraints imposed in [20] are lifted and the most generic relations will be derived, for the formulation of Eqs. (1) and (3).

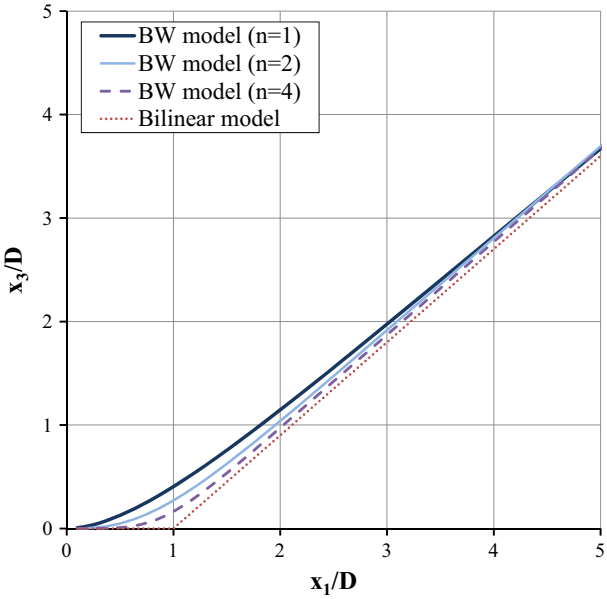

Fig. 3 Normalized residual deformation of a system with $A = 1, \beta = 0.75, \gamma = 0.25, k = 25, D = 0.15, \alpha = 0.10$ in a loading/unloading cycle as a function of the maximum displacement during loading

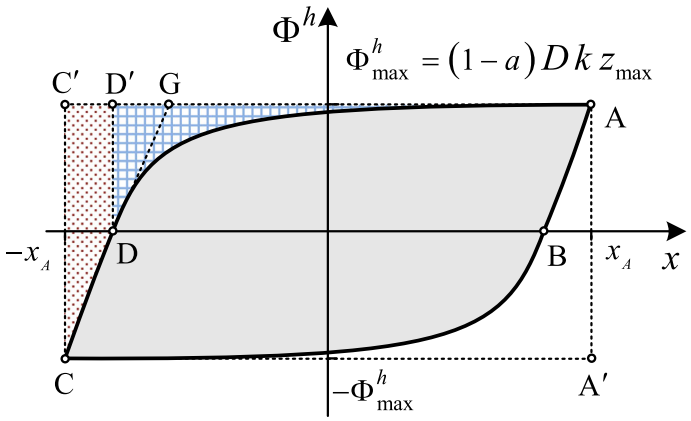

Fig. 4 Steady-state response of hysteretic spring under symmetric wave T-periodic excitation

4.2 Solution

4.2.1 General outline

The dissipated energy is expressed by the area enclosed by hysteretic loops. The elastic spring of the Bouc–Wen model does not dissipate energy, nor does it store energy in a closed displacement loop, and will be ignored.

In our case, the displacement amplitude is common in both directions (Fig. 4). Points A and C signify sign reversal of velocity $\dot{x}$, whereas points B and D signify sign reversal of hysteretic parameter z. The maximum value of the latter, occurring at point A, corresponds to the maximum displacement. Making use of symmetry, it follows that $x_A = x_{\max} = -x_C$ and $z_A = -z_C$, where the subscript denotes the corresponding point of the hysteretic loop. Considering the transition from point C to point A and employing Eq. (5), we obtain:

$$\frac{x_{\max}}{D} = \frac{z_A}{2A}\left({}_2F_1\left(1, \frac{1}{n}, 1+\frac{1}{n}; \frac{\gamma-\beta}{A} z_A^n\right) + {}_2F_1\left(1, \frac{1}{n}, 1+\frac{1}{n}; \frac{\beta+\gamma}{A} z_A^n\right)\right) \tag{27}$$

where, z_A is the unknown maximum observed value of hysteretic parameter z, corresponding to the steady-state response under symmetric excitation of amplitude $x_{\max}$. There exist several analytical expressions of z_A for

Table 2 Analytical expressions for coefficient $\bar{k}^*_{CD} = k^*_{CD}\big|_{z_A=z_{\max}}$ for specific values of n

n	$\bar{k}^*_{CD}$
1	$\frac{\beta-\gamma-2\gamma\ln\left(\frac{2\beta}{\beta+\gamma}\right)}{(\beta-\gamma)^2}$
2	$\frac{2\sqrt{\gamma-\beta}\,\operatorname{atanh}\left(\sqrt{1-\frac{2\beta}{\beta+\gamma}}\right)-\sqrt{\beta+\gamma}\ln\left(\frac{2\beta}{\beta+\gamma}\right)}{2\sqrt{A}(\gamma-\beta)}$
4	$\frac{\sqrt[4]{\gamma-\beta}\left(\operatorname{atan}\left(\sqrt[4]{1-\frac{2\beta}{\beta+\gamma}}\right)+\operatorname{atanh}\left(\sqrt[4]{1-\frac{2\beta}{\beta+\gamma}}\right)\right)+\sqrt[4]{\beta+\gamma}\,\operatorname{atanh}\left(\sqrt{1-\frac{2\beta}{\beta+\gamma}}\right)}{2\sqrt[4]{A^3}\sqrt{\gamma-\beta}}$

specific model parameters. In general, however, numerical evaluation must be employed. In similar manner, as in the preceding section, the Van Wijngaarden–Dekker–Brent method [24] can be employed which converges rapidly. If root bracketing with $z_A \in [0, z_{\max} - \varepsilon]$ fails, then full yield is assumed and $z_A = z_{\max}$.

Having evaluated z_A, the dissipated energy during a complete cycle can be expressed in terms of it. The enclosed area is given by:

$$E = \oint \Phi^h dx \tag{28}$$

For softening models, such as Class I and II models, attempting to change variable and integrate in terms of z leads to a formulation that is numerically unstable, as analyzed in [20]. A method that eliminates this problem is to evaluate the complementary areas, i.e., the dashed areas of Fig. 4, and subtract them from the outer rectangle. Making use of symmetry, the dissipated energy is then expressed as follows:

$$E = 4\Phi^h_{\max} x_{\max} - 2\int_{x_C}^{x_A} \left(\Phi^h_{\max} - \Phi^h\right) dx \tag{29}$$

Where, the maximum possible value of $\Phi^h_{\max} = (1-a)\,D\;k\;z_{\max}$ has been used, although this is not mandatory.

4.2.2 Unloading branch CD

Restricting attention to segment CD, the complementary area is given by:

$$E_{D'C'CD} = \Phi^h_{\max}\, D \int_{-z_A}^{0} \frac{1 - z/z_{\max}}{A - (\gamma-\beta)\,(-z)^n} dz \tag{30}$$

This expression is simplified as $E_{D'C'CD} = \Phi^h_{\max}\; D\; k^*_{CD}$, where the coefficient k^*_{CD} can be expressed in its general form as follows:

$$k^*_{CD} = \frac{z_A}{A}\left({}_2F_1\left(1, \frac{1}{n}, 1+\frac{1}{n}; \frac{\gamma-\beta}{A} z_A^n\right) + \frac{z_A}{2z_{\max}}\,{}_2F_1\left(1, \frac{2}{n}, 1+\frac{2}{n}; \frac{\gamma-\beta}{A} z_A^n\right)\right) \tag{31}$$

In the common case of fully yielding systems, we can substitute $z_A = z_{\max}$ and Eq. (31) is simplified as:

$$\bar{k}^*_{CD} = \frac{z_{\max}}{A}\left({}_2F_1\left(1, \frac{1}{n}, 1+\frac{1}{n}; \frac{\gamma-\beta}{\beta+\gamma}\right) + \frac{1}{2}\,{}_2F_1\left(1, \frac{2}{n}, 1+\frac{2}{n}; \frac{\gamma-\beta}{\beta+\gamma}\right)\right) \tag{32}$$

There exist several elegant analytical simplifications of Eq. (32) for specific values of n. These are summarized in Table 2, where $\ln(\cdot)$ is the natural logarithm and $\operatorname{atan}(\cdot)$ is the inverse tangent.

In the special case of $\beta = \gamma$, the unloading branches are straight lines and Eq. (31) is simplified as:

$$\hat{k}^*_{CD} = \frac{z_A\,(z_A + 2z_{\max})}{2A\;z_{\max}} \tag{33}$$

Finally, when both $\beta = \gamma$ and the system yields fully, Eq. (31) is simplified as:

$$\hat{\bar{k}}^*_{CD} = \frac{3z_{\max}}{2A} \tag{34}$$

Table 3 Analytical expressions for coefficient $\bar{k}^*_{DA} = \lim_{z_A \to z^-_{\max}} \left(k^*_{DA}\right)$ for specific values of n

n	$\bar{k}^*_{DA}$
$\frac{1}{2}$	$\frac{5A}{3(\beta+\gamma)^2}$
1	$\frac{1}{\beta+\gamma}$
$\frac{3}{2}$	$\frac{2\left(\sqrt{3}\pi-9\right)}{9\sqrt[3]{A(\beta+\gamma)^2}}$
2	$\frac{\ln(2)}{\sqrt{A(\beta+\gamma)}}$
3	$\frac{\pi}{3\sqrt{3}\sqrt[3]{A^2(\beta+\gamma)}}$
4	$\frac{\pi+\ln(4)}{8\sqrt[4]{A^3(\beta+\gamma)}}$
6	$\frac{\sqrt{3}\pi+\ln(64)}{18\sqrt[6]{A^5(\beta+\gamma)}}$
12	$\sqrt[12]{\frac{A}{\beta+\gamma}}\frac{2\pi+\ln(4)+\sqrt{3}\ln\left(7+4\sqrt{3}\right)}{24A}$

4.2.3 Loading branch DA

Following similar formulation for segment DA, the complementary area is evaluated as:

$$E_{AD'D} = \Phi^h_{\max} D \int_0^{z_A} \frac{1 - z/z_{\max}}{A - (\beta+\gamma)\, z^n} dz \tag{35}$$

This expression is simplified as $E_{AD'D} = \Phi^h_{\max} D\ k^*_{DA}$, where the coefficient k^*_{DA} can be expressed in its general form as follows:

$$k^*_{DA} = \frac{z_A}{A}\left({}_2F_1\left(1, \frac{1}{n}, 1+\frac{1}{n}; \frac{\beta+\gamma}{A} z_A^n\right) - \frac{z_A}{2z_{\max}}\,{}_2F_1\left(1, \frac{2}{n}, 1+\frac{2}{n}; \frac{\beta+\gamma}{A} z_A^n\right)\right) \tag{36}$$

In case of fully yielding systems, it follows that $z_A \to z^-_{\max}$ and the limit of Eq. (31) must be evaluated. Proper evaluation techniques are provided in the Appendix C. Several elegant analytical solutions also exist for the coefficient $\bar{k}^*_{DA} = \lim\limits_{z_A \to z^-_{\max}} \left(k^*_{DA}\right)$, as summarized in Table 3.

4.2.4 Full cycle

Having evaluated k^*_{CD} and k^*_{DA}, the dissipated energy is given by the simple expression:

$$E = \Phi^h_{\max} D \left(4\frac{x_{\max}}{D} - 2\left(k^*_{CD} + k^*_{DA}\right)\right) \tag{37}$$

In case the system yields fully ($z_A \to z^-_{\max}$), then the dissipated energy can be evaluated by:

$$\bar{E} = \Phi^h_{\max} D \left(4\frac{x_{\max}}{D} - 2\left(\bar{k}^*_{CD} + \bar{k}^*_{DA}\right)\right) \tag{38}$$

In this case, we can summarize some simplified expressions for $n = 1$, $n = 2$ and $n = 4$, as follows:

$$\frac{\bar{E}_{n=1}}{\Phi^h_{\max} D} = 4\frac{x_{\max}}{D} - 2\left(\frac{1}{\beta+\gamma} + \frac{1}{\beta-\gamma} - \frac{2\gamma \ln\left(\frac{2\beta}{\beta+\gamma}\right)}{(\beta-\gamma)^2}\right) \tag{39}$$

$$\frac{\bar{E}_{n=2}}{\Phi^h_{\max} D} = 4\frac{x_{\max}}{D} - \frac{2}{\sqrt{A}}\left(\frac{\operatorname{atanh}\left(\sqrt{\frac{\gamma-\beta}{\beta+\gamma}}\right)}{\sqrt{\gamma-\beta}} + \frac{(\beta-\gamma)\ln(4) + (\beta+\gamma)\ln\left(\frac{2\beta}{\beta+\gamma}\right)}{2(\beta-\gamma)\sqrt{\beta+\gamma}}\right) \tag{40}$$

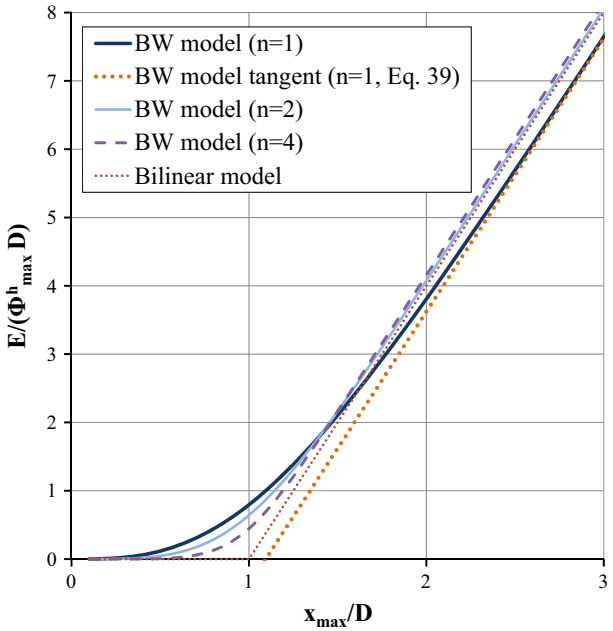

Fig. 5 Normalized dissipated energy of a system with $A = 1$, $\beta = 0.75$, $\gamma = 0.25$ under symmetric wave T-periodic excitation

$$\frac{\bar{E}_{n=4}}{\Phi^h_{\max} D} = 4\frac{x_{\max}}{D} - \frac{1}{4\sqrt[4]{A^3}} \times \left(4\frac{\sqrt[4]{\gamma-\beta}\left(\operatorname{atan}\left(\sqrt[4]{\frac{\gamma-\beta}{\beta+\gamma}}\right) + \operatorname{atanh}\left(\sqrt[4]{\frac{\gamma-\beta}{\beta+\gamma}}\right)\right) + \sqrt[4]{\beta+\gamma}\operatorname{atanh}\left(\sqrt{\frac{\gamma-\beta}{\beta+\gamma}}\right)}{\sqrt{\gamma-\beta}} + \frac{\pi + \ln(4)}{\sqrt[4]{(\beta+\gamma)}} \right) \tag{41}$$

Finally, if the system yields fully and $\beta = \gamma$, the corresponding expressions are further simplified, as follows:

$$\frac{\hat{\bar{E}}_{n=1}}{\Phi^h_{\max} D} = 4\frac{x_{\max}}{D} - \frac{5}{2\beta} \tag{42}$$

$$\frac{\hat{\bar{E}}_{n=2}}{\Phi^h_{\max} D} = 4\frac{x_{\max}}{D} - \frac{3 + \ln(4)}{\sqrt{2A\beta}} \tag{43}$$

$$\frac{\hat{\bar{E}}_{n=4}}{\Phi^h_{\max} D} = 4\frac{x_{\max}}{D} - \frac{\pi + 12 + \ln(4)}{4\sqrt[4]{2A^3\beta}} \tag{44}$$

A worked example, demonstrating the evaluation of the dissipated energy of Bouc–Wen model, is provided in the Appendix F.

4.3 Parametric studies

Based on the derived relations, we can perform parametric studies of the dissipated energy of the Bouc–Wen model. In Fig. 5, we show the normalized dissipated energy $E/\left(\Phi^h_{\max} D\right)$ as a function of the normalized displacement amplitude $x_{\max}/D$ for a system with $A = 1, \beta = 0.75, \gamma = 0.25$ and specific values of n. Note that $A/(\beta + \gamma) = 1$ which yields a system with well-defined mechanical properties [30]. In this case, $z_{\max} = 1$, irrespectively of n. The corresponding bilinear model is also included in Fig. 5, which yields no dissipated energy in the elastic regime ($x_{\max} \leq D$). Since $\beta > \gamma$ (Class I model), the hysteretic loops are rounded and the bilinear model either overestimates or slightly underestimates the dissipated energy as $x_{\max}/D$

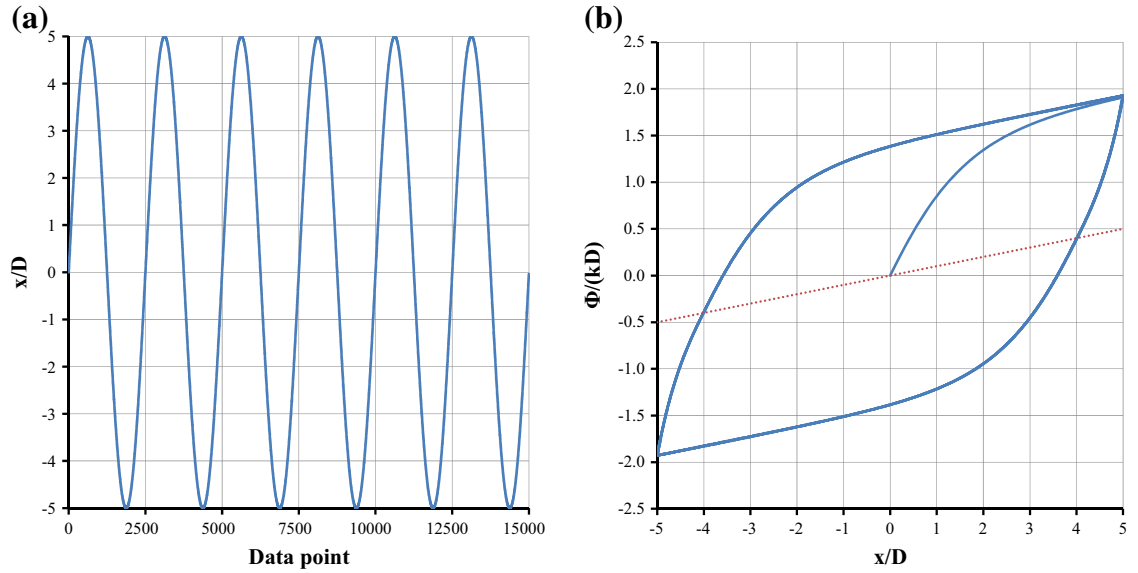

Fig. 6 **a** Imposed displacement pattern **b** response of a system with $A = 1, \beta = 0.75, \gamma = -0.25, k = 25, D = 0.15$ and $n = 1.5$. The *dotted line* signifies the response of the linear spring

is increased. However, if $\beta \leq \gamma$, the bilinear model always overestimates the dissipated energy, since either the unloading branches are straight lines (for $\beta = \gamma$), or the hysteretic loops take the form of a slim "S" (for $\beta < \gamma$, Class II). Note also that Eqs. (39)–(44) are linear with respect to the normalized amplitude $x_{\max}/D$, and represent the tangent of the exact Eq. (37) as $x_{\max}/D$ is increased. Only the tangent for $n = 1$ is included in Fig. 5, for reasons of clarity.

5 Conclusions

A previous study [20] regarding the response and dissipated energy of the Bouc–Wen model is extended considerably. New analytical and numerical solutions are derived based on a general model formulation without any parameter constraints. These solutions provide insight into the inner workings of the model; they are used herein to address issues such as the inexistence of elastic domain or the calculation of the residual deformation in a loading-unloading cycle. It is also shown that other results found in the literature are related to the ones presented herein, with the latter being in an advantageous form for analytical and numerical evaluation.

Appendix A: Loop tracing

Consider a system with $A = 1, \beta = 0.75, \gamma = -0.25, k = 25, D = 0.15, a = 0.1$ and $n = 1.5$ (Class I), with consistent units. The system is subjected to a prescribed sinusoidal pattern with amplitude equal to $5D$, as shown in Fig. 6a, where the vertical axis has been normalized. The hysteretic loop is independent of the period of excitation, the rate of loading, or even the actual pattern; the same result is also obtained e.g., with a triangular pattern. In fact, the only information required is the sequence of local minima and maxima of x, i.e., $x = 0 \to 5D \to -5D \to 5D \to \cdots$. The resulting hysteretic loop is shown in Fig. 6b, where the dotted line signifies the linear response.

When z at the end of the transition is known, solving Eq. (5) for x produces:

$$x = D\left(\frac{z}{A} {}_2F_1\left(1, \frac{1}{n}, 1 + \frac{1}{n}; \frac{q}{A}|z|^n\right)\Big|_{z_0}^{z} \right) + x_0 \tag{45}$$

When x is known but z is not, we rewrite Eq. (5) to define an auxiliary function for the bisection method:

$$R(x, x_0, z, z_0, q) = \frac{z}{A} {}_2F_1\left(1, \frac{1}{n}, 1 + \frac{1}{n}; \frac{q}{A}|z|^n\right)\Big|_{z_0}^{z} - \frac{x - x_0}{D} \tag{46}$$

For the root bracketing, we evaluate $z_{\max}$ from Eq. (7) as $z_{\max} \cong 1.5874$. The loops are traced as follows:

Step 1 (DA branch): $x_0 = 0, z_0 = 0, x = 0.75, z$ is unknown. Low value of $z = 0$ produces $R\,(5D, 0, z, 0, \beta + \gamma) = -5$. High value of $z = z_{\max} - 10^{-6}$ produces $R\,(5D, 0, z, 0, \beta + \gamma) \cong 10.4646$. Value of $z \cong 1.56776$ is obtained by root bracketing and bisection, with $\Phi/(kD) = 1.91098$.

Step 2 (AB branch): $x_0 = 5D, z_0 = 1.56776, z = 0, x$ is unknown and evaluated directly by Eq. (45) with $q = \gamma - \beta$ as $x \cong 0.602919$, with $x/D = 4.01946$.

Step 3 (BC branch): $x_0 = 0.602919, z_0 = 0, x = -5D, z$ is unknown. High value of $z = 0$ produces $R\,(-5D, 0.602919, z, 0, \beta + \gamma) \cong 9.01946$. Low value of $z = -\left(z_{\max} - 10^{-6}\right)$ produces $R\,(-5D, 0.602919, z, 0, \beta + \gamma) \cong -6.44517$. Value of $z \cong -1.58696$ is obtained by root bracketing and bisection, with $\Phi/(kD) = -1.92826$.

Step 4 (CD branch): $x_0 = -5D, z_0 = -1.58696, z = 0, x$ is unknown and evaluated directly by Eq. (45) with $q = \gamma - \beta$ as $x \cong -0.601953$, with $x/D = -4.01302$.

Step 5 (DA branch): $x_0 = -0.601953, z_0 = 0, x = 5D, z$ is unknown. Low value of $z = 0$ produces $R\,(5D, -0.601953, z, 0, \beta + \gamma) \cong -9.01302$. High value of $z = z_{\max} - 10^{-6}$ produces $R\,(5D, -0.601953, z, 0, \beta + \gamma) = 6.45161$. Value of $z \cong 1.58696$ is obtained by root bracketing and bisection, with $\Phi/(kD) = 1.92826$.

Even from the first load cycle, the response converges in the symmetric hysteretic loop $(x, \Phi/(kD)) \cong (5D, 1.92826) \rightleftarrows (-5D, -1.92826)$ (Fig. 6b). The proof that oscillation between two opposite values of z traces the same loop precisely is given in the Appendix B.

When $n = 1$ or $n = 2$, the procedure is facilitated considerably. Instead of using Eq. (46) for root bracketing and bisection, one can use directly Eqs. (9) or (11).

Appendix B: Symmetric hysteretic loop

We will prove that, beginning at point $P^+\left(x^+, z^+\right)$, a hysteretic loop for which z varies in the sequence $z^+ \to -z^+ \to z^+$ will be guided to P^+ exactly.

We assume that the final point is $\hat{P}^+\left(\hat{x}^+, z^+\right) \neq P^+$. The hysteretic loop can be analyzed into the sequence $P^+ \to P_1\,(x_1, 0) \to P_2\left(x_2, -z^+\right) \to P_3\,(x_3, 0) \to \hat{P}^+$. By successive application of Eq. (5), one obtains:

$$\frac{x_1 - x^+}{D} = 0 - \frac{z^+}{A}\,{}_2F_1\left(1, \frac{1}{n}, 1 + \frac{1}{n}; \frac{(\gamma - \beta)}{A}\left|z^+\right|^n\right) \tag{47}$$

$$\frac{x_2 - x_1}{D} = -\frac{z^+}{A}\,{}_2F_1\left(1, \frac{1}{n}, 1 + \frac{1}{n}; \frac{(\beta + \gamma)}{A}\left|-z^+\right|^n\right) - 0 \tag{48}$$

$$\frac{x_3 - x_2}{D} = 0 - \left[-\frac{z^+}{A}\,{}_2F_1\left(1, \frac{1}{n}, 1 + \frac{1}{n}; \frac{(\gamma - \beta)}{A}\left|-z^+\right|^n\right)\right] \tag{49}$$

$$\frac{\hat{x}^+ - x_3}{D} = \frac{z^+}{A}\,{}_2F_1\left(1, \frac{1}{n}, 1 + \frac{1}{n}; \frac{(\beta + \gamma)}{A}\left|z^+\right|^n\right) - 0 \tag{50}$$

By adding Eqs. (47)–(50) by parts, one obtains $\hat{x}^+ = x^+$. Thus, $\hat{P}^+ = P^+$.

Appendix C: Evaluation of Gauss' hypergeometric function

In this study, one is interested in the evaluation of ${}_2F_1\,(a, b, c; w)$ for real values of $w \in (-\infty, 1)$ with $c = a + b$.

The hypergeometric function is the analytical continuation of the hypergeometric series [31]:

$${}_2F_1\,(a, b, c; w) = 1 + \frac{ab}{1!c}z + \frac{a\,(a+1)\,b\,(b+1)}{2!c\,(c+1)}z^2 + \cdots = \sum_{n=0}^{\infty}\frac{(a)_n\,(b)_n}{(c)_n}\frac{w^n}{n!} \tag{51}$$

where, $(\cdot)_n$ is Pochhammer's symbol, defined as $(w)_n = w\,(w+1)\cdots(w+n-1)$ with $(w)_0 = 1$, and $n!$ the factorial of n.

Series (51) converges for all $|w| < 1$, but its rate of convergence is satisfactory only for $|w| \leq 1/2$ [24]. Thus, for $w \in (-1/2, 1/2)$, evaluation is performed directly by Eq. (51).

For $w \in (1/2, 1)$, a linear transformation is required. In the cases presented herein, $c = a + b$ and hence the following formula is used [31, eq. 15.3.10]:

$$
\begin{aligned}
{}_2F_1(a, b, a+b; w) = {} & \frac{\Gamma(a+b)}{\Gamma(a)\,\Gamma(b)} \sum_{n=0}^{\infty} \frac{(a)_n\,(b)_n}{(n!)^2} \\
& \times [2\psi(n+1) - \psi(a+n) - \psi(b+n) - \ln(1-w)]\,(1-w)^n
\end{aligned} \tag{52}
$$

where, $\Gamma(\cdot)$ is the gamma function and $\psi(\cdot)$ the psi (digamma) function. These functions are treated in Appendix D and E, respectively. In general, Eq. (52) exhibits satisfactory rate of convergence even when evaluating $\lim_{w \to 1^-} {}_2F_1(a, b, c; w)$.

Finally, for $w \in (-\infty, -1/2)$, the following linear transformation is used [31, eq. 15.3.4]:

$$
{}_2F_1(a, b, c; w) = (1-w)^{-a}\, {}_2F_1\left(a, c-b, c; \frac{w}{w-1}\right) \tag{53}
$$

The new function evaluation falls into one of the cases covered by Eqs. (51) and (52).

Appendix D: Evaluation of gamma function

The gamma function can be defined for $\mathrm{Re}\, z > 0$ by Euler's integral [31, eq. 6.1.1]:

$$
\Gamma(z) = \int_0^{\infty} t^{z-1} e^{-t}\, dt \tag{54}
$$

where, in general, z is complex. $\Gamma(z)$ is single-valued and analytic everywhere in the complex plane except at $z = k$, $k = 0, -1, -2, \ldots$, where it possesses simple poles.

The evaluation of the gamma function is most commonly accomplished using Lanczos algorithm [32], which corrects Stirling's approximation with contributions from the function's poles. It requires $O(-\log \varepsilon)$ time, independent of z, to calculate $z!$ with a relative error ε. Note that usually $\ln \Gamma(z)$ is evaluated instead of $\Gamma(z)$, because overflow is unavoidable even with moderate values of z. The evaluation of gamma function can also be accomplished using Spouge's algorithm [33]. This algorithm has the same form and requires slightly more computations as compared to Lanczos'. However, it can be used for the evaluation of psi (digamma) function as well, while the error is easier to estimate. For these reasons, it will described in brief.

According to Spouge's algorithm, the relative error ε for computing $\Gamma(z+1)$ with $\mathrm{Re}\, z > 0$ is bounded by the expression [33]:

$$
|\varepsilon| \leq a^{-1/2}\, (2\pi)^{-(a+1/2)} \tag{55}
$$

where, $a \geq 3$ controls the number of terms of the approximation. Herein, we choose $\varepsilon_{\max} = 10^{-10}$. Solving (55) numerically for a yields $11.3772\ldots$, thus $\lceil a \rceil = 12$, where $\lceil a \rceil$ is the ceiling of a, denoting the unique integer satisfying $\lceil a \rceil - 1 < a \leq \lceil a \rceil$. The coefficients c_k of Spouge's algorithm are given by [33]:

$$
\begin{aligned}
c_0 &= 1 \\
c_k &= (2\pi)^{-\frac{1}{2}}\, \frac{(-1)^{k-1}}{(k-1)!}\, (-k+a)^{k-\frac{1}{2}}\, e^{-k+a},\ k \in \{1, 2, \ldots, \lceil a \rceil - 1\}
\end{aligned} \tag{56}
$$

Note that the evaluation of the coefficients is much simpler than those of Lanczos [32]. For $\lceil a \rceil = 12$, these are:

$$
\begin{aligned}
c_0 &= 1 \\
c_1 &= 79{,}221.98306133379 \\
c_2 &= -277{,}878.4609602073 \\
c_3 &= 392{,}768.5278126612
\end{aligned}
$$

$$
\begin{aligned}
c_4 &= -287{,}031.5426615348\\
c_5 &= 115{,}798.0850399489\\
c_6 &= -25{,}546.27531493711\\
c_7 &= 2{,}873.128215161947\\
c_8 &= -141.6143919456524\\
c_9 &= 2.258414498459323\\
c_{10} &= -5.881944949935368 \times 10^{-3}\\
c_{11} &= 2.988419178293727 \times 10^{-7}
\end{aligned} \tag{57}
$$

$\Gamma(z)$ is thus given by the following expression:

$$
\begin{aligned}
\Gamma(z) = {} & (z+\lceil a\rceil)^{z+\frac{1}{2}}\, e^{-(z+\lceil a\rceil)}\\
& \times \frac{\sqrt{2\pi}}{z}\left[c_0 + \frac{c_1}{z+1} + \frac{c_2}{z+2} + \cdots + \frac{c_{\lceil a\rceil-1}}{z+\lceil a\rceil-1} + \varepsilon\right],\ \mathrm{Re}\, z > 0
\end{aligned} \tag{58}
$$

Finally, evaluation of $\Gamma(z)$ for $\mathrm{Re}\, z < 0$ can be accomplished using the reflection formula [31, eq. 6.1.17]:

$$
\Gamma(z) = \frac{\pi}{\sin(\pi z)\,\Gamma(1-z)} \tag{59}
$$

Appendix E: Evaluation of psi (digamma) function

The psi (digamma) function $\psi(\cdot)$ is defined as the logarithmic derivative of $\Gamma(z)$, defined everywhere in the complex plane except at $z = k, k = 0, -1, -2, \ldots$:

$$
\psi(z) = \frac{d}{dz}\ln\Gamma(z) = \frac{\Gamma'(z)}{\Gamma(z)} \tag{60}
$$

Its evaluation can be accomplished efficiently using Spouge's algorithm [33]. Let $D = \left(1-(2/3)^{1/2}(2\pi)^{-2}\right)^{-1} = 1.02111\ldots$ The absolute error for computing $\psi(z+1)$ with $\mathrm{Re}\, z > 0$ and $a \geq 3/2$ is bounded by the expression [33]:

$$
|\varepsilon| \leq D\ln(2a)\, a^{-1/2}(2\pi)^{-(a+1/2)} \tag{61}
$$

We choose $\varepsilon_{\max} = 10^{-10}$. Solving (61) numerically for a yields $11.993\ldots$, therefore $\lceil a\rceil = 12$, which coincides with the case described in Appendix D. Thus, the particular coefficients c_k are given by Eq. (57) and $\psi(z)$ is evaluated as:

$$
\begin{aligned}
\psi(z) = {} & \ln(z+\lceil a\rceil) - (\lceil a\rceil - 1/2)(z+\lceil a\rceil)^{-1}\\
& - \frac{\frac{c_1}{(z+1)^2} + \frac{c_2}{(z+2)^2} + \cdots + \frac{c_{\lceil a\rceil-1}}{(z+\lceil a\rceil-1)^2}}{c_0 + \frac{c_1}{z+1} + \frac{c_2}{z+2} + \cdots + \frac{c_{\lceil a\rceil-1}}{z+\lceil a\rceil-1}} - \frac{1}{z} + \varepsilon,\ \mathrm{Re}\, z > 0
\end{aligned} \tag{62}
$$

where, the recurrence formula $\psi(z+1) = \psi(z) + 1/z$ [31, eq. 6.3.5] was employed. Finally, evaluation of $\psi(z)$ for $Re\ z < 0$ can be accomplished using the reflection formula [31, eq. 6.3.7]:

$$
\psi(z) = \psi(1-z) - \frac{\pi}{\tan(\pi z)} \tag{63}
$$

Appendix F: Evaluation of dissipated energy in a closed displacement cycle

Consider the system of Fig. 6b. Using Eq. (7), we obtain $z_{\max} \cong 1.58740$ and therefore $\Phi^h_{\max} = 5.35748$. Using root bracketing for z_A in the range $[0, 1.58740 - \varepsilon]$, we evaluate $z_A \cong 1.58696$ from Eq. (27). Note that this coincides with the final value of z, evaluated in the corresponding example, when the system settled in the steady-state response. Next, $k^*_{CD} = 1.38652$ and $k^*_{DA} = 1.25502$ from Eqs. (31) and (36), respectively. Finally, $E = 11.82680$ from Eq. (37).

References

1. Visintin, A.: Differential Models of Hysteresis. Springer, Berlin (1994)
2. Bouc, R.: Forced vibration of mechanical systems with hysteresis. In: Proceedings of 4th Conference on Non-linear Oscillation, Prague, Czechoslovakia (1967)
3. Wen, Y.K.: Method for random vibration of hysteretic systems. J. Eng. Mech. Div. **102**(2), 249–263 (1976)
4. Saatcioglu, M., Ozcebe, G.: Response of reinforced concrete columns to simulated seismic loading. ACI Struct. J. **86**(1), 3–12 (1989)
5. Triantafyllou, S.P., Koumousis, V.K.: Small and large displacement dynamic analysis of frame structures based on hysteretic beam elements. J. Eng. Mech. **138**(1), 36–49 (2011)
6. Lefas, I.D., Kotsovos, M.D.: Strength and deformation characteristics of reinforced concrete walls under load reversals. ACI Struct. J. **87**(6), 716–726 (1990)
7. Madan, A., Reinhorn, A.M., Mander, J.B.: Fiber-element model of posttensioned hollow block masonry shear walls under reversed cyclic lateral loading. J. Struct. Eng. **134**(7), 1101–1114 (2008)
8. Sireteanu, T., Giuclea, M., Mitu, A.M.: Identification of an extended Bouc–Wen model with application to seismic protection through hysteretic devices. Comput. Mech. **45**(5), 431–441 (2010)
9. Quaranta, G., Marano, G.C., Greco, R., Monti, G.: Parametric identification of seismic isolators using differential evolution and particle swarm optimization. Appl. Soft. Comput. doi:10.1016/j.asoc.2014.04.039 (2014)
10. Foliente, G.C.: Hysteresis modeling of wood joints and structural systems. J. Struct. Eng. **121**(6), 1013–1022 (1995)
11. Gerolymos, N., Gazetas, G.: Static and dynamic response of massive caisson foundations with soil and interface nonlinearities—validation and results. Soil Dyn. Earthq. Eng. **26**, 377–394 (2006)
12. Kwok, N.M., Ha, Q.P., Nguyen, T.H., Li, J., Samali, B.: A novel hysteretic model for magnetorheological fluid dampers and parameter identification using particle swarm optimization. Sens. Actuators A **132**, 441–451 (2006)
13. Talatahari, S., Kaveh, A., Rahbari, N.M.: Parameter identification of Bouc–Wen model for MR fluid dampers using adaptive charged system search optimization. J. Mech. Sci. Technol. **26**(8), 2523–2534 (2012)
14. Hoon, W., Yoon, Y.K., Haeil, J., Gwang, N.L.: Nonlinear rate-dependent stick-slip phenomena: modeling and parameter estimation. Int. J. Solids Struct. **38**, 1415–1431 (2001)
15. Gunstona, T.P., Rebelleb, J., Griffina, M.J.: A comparison of two methods of simulating seat suspension dynamic performance. J. Sound Vib. **278**, 117–134 (2004)
16. Ismail, M., Ikhouane, F., Rodellar, J.: The hysteresis Bouc–Wen model, a survey. Arch. Comput. Methods Eng. **16**(2), 161–188 (2009)
17. Triantafyllou, S.P., Koumousis, V.K.: Bouc–Wen type hysteretic plane stress element. J. Eng. Mech. **138**(3), 235–246 (2011)
18. Triantafyllou, S.P., Koumousis, V.K.: An hysteretic quadrilateral plane stress element. Arch. Appl. Mech. **82**(10-11), 1675–1687 (2012)
19. Ülker-Kaustell, M., Karoumi, R.: Influence of rate-independent hysteresis on the dynamic response of a railway bridge. Int. J. Rail Transp. **1**(4), 237–257 (2013)
20. Charalampakis, A.E., Koumousis, V.K.: On the response and dissipated energy of Bouc–Wen hysteretic model. J. Sound Vib. **309**, 887–895 (2008)
21. Charalampakis, A.E., Koumousis, V.K.: A Bouc–Wen model compatible with plasticity postulates. J. Sound Vib. **322**, 954–968 (2009)
22. Ikhouane, F., Rodellar, J.: On the hysteretic Bouc–Wen model, Part I: forced limit cycle characterization. Nonlinear Dyn. **42**, 63–78 (2005)
23. Dominguez, A., Sedaghati, R., Stiharu, I.: Modelling the hysteresis phenomenon of magnetorheological dampers. Smart Mater. Struct. **13**, 1351–1361 (2004)
24. Press, W.H., Teukolsky, S.A., Vetterling, W.T., Flannery, B.P.: Numerical Recipes in C++: The Art of Scientific Computing. Cambridge University Press, Cambridge (2002)
25. Ikhouane, F., Rodellar, J., Hurtado, J.E.: Analytical characterization of hysteresis loops described by the Bouc–Wen model. Mech. Adv. Mater. Struct. **13**, 463–472 (2006)
26. Valanis, K.C.: A theory of viscoplasticity without a yield surface. Part I: general theory. Arch. Mech. **23**(4), 517–533 (1971)
27. Bažant, Z.: Endochronic inelasticity and incremental plasticity. Int. J. Solids Struct. **14**, 691–714 (1978)
28. Weisstein, E.W.: Lambert W-Function. MathWorld-A Wolfram Web Resource. http://mathworld.wolfram.com/LambertW-Function.html. Accessed 18/07/2012 (2012)
29. Sgobba, S., Marano, G.C.: Optimum design of linear tuned mass dampers for structures with nonlinear behavior. Mech. Syst. Signal Process. **24**, 1739–1755 (2010)
30. Constantinou, M.C., Adnane, M.A.: Dynamics of Soil-Base-Isolated Structure Systems: Evaluation of Two Models for Yielding Systems. Report to NSAF, Department of Civil Engineering, Drexel University, Philadelphia (1987)
31. Abramowitz, M., Stegun, I.A.: Handbook of Mathematical Functions. Washington: National Bureau of Standards; reprinted by Dover Publications, New York (1972)
32. Lanczos, C.: A precision approximation of the gamma function. J. Soc. Ind. Appl. Math. Ser. B Numer. Anal. **1**, 86–96 (1964)
33. Spouge, J.L.: Computation of the gamma, digamma, and trigamma functions. J. Soc. Ind. Appl. Math. **31**(3), 931–944 (1994)